Electromechanical Energy Conversion Systems (EECS)
Niroo Research Institute (NRI)
Vol. 4, No. 1, Spring 2025, pp. 36- 41
DOI: 10.30503/EECS.2025.494192.1066
Original Article

Innovative Design Optimization of Mover Saliency in Tubular Variable Reluctance Resolvers via MEC

Farid Tootoonchian [1*], Fateme Zare [2]

Abstract

Resolvers are essential position sensors used to determine rotational and linear positions. Based on their structure, they are classified into two main types: wound rotor resolvers and variable reluctance resolvers. This paper analyzes the performance of a tubular variable reluctance resolver using the Magnetic Equivalent Circuit (MEC) method. The proposed model's accuracy is validated by comparing its results with those obtained from 3D finite element simulations.
Furthermore, various configurations of the tubular variable reluctance resolver are examined, including the inner stator long mover, inner stator short mover, and outer stator long mover. Since the number of saliencies in the variable reluctance section significantly influences resolver performance, its effect on accuracy is analyzed for a fixed number of slots. The optimized configuration is identified as the inner stator long mover with five saliencies. Finally, the optimal configuration with the lowest error is experimentally tested, and the results from the fabricated prototype confirm the validity of the conducted studies.

Keywords: Linear Resolver, Tubular Resolver, Variable Reluctance Resolver, Magnetic Equivalent Circuit (MEC), End Effect.

Received Date: 2024-12-15; Revised Date: 2025-02-09 ; Accepted Date: 2025-04-28

1. INTRODUCTION

Position sensors are critical components in control systems. Among these, resolvers are widely used due to their high reliability, robustness in noisy industrial environments, and resistance to temperature variations, outperforming sensors like encoders [1]-[2]. Resolvers, comprising a rotor and a stator, are categorized into wound rotor and variable reluctance types. In wound rotor resolvers, both the rotor and stator include windings designed to produce a sinusoidal variation in mutual inductance between the excitation and signal windings [3]-[4]. In variable reluctance resolvers, the excitation and signal windings are located in the stator, while the rotor lacks windings. Sinusoidal mutual inductance is achieved through the rotor's geometric design [5]-[6].
Variable reluctance resolvers are further divided into two types: those with variable air-gap length and those with variable cross-section [7]-[8]-[9]-10]. It is worth mentioning that both wound rotor and variable reluctance resolvers can be designed in radial flux and axial flux constructions [11]-[12]-13]. Both types can be applied in linear resolver structures. Considering the structure of variable reluctance resolvers, their manufacturing process is more straightforward, and they are generally more reliable. However, wound rotor resolvers are typically more accurate. Reference [14] examines flat wound mover resolvers, while [15] introduces linear variable reluctance resolvers with a variable air-gap length. Due to the computational cost of finite element simulations, employing analytical methods for studying the performance of electrical machines is common [16]-[17]. In this regard, the performance of these resolvers has been analyzed using the magnetic equivalent circuit (MEC) method and winding functions [18]-[19]. [18] proposes a method for compensating the end effect in a variable reluctance linear resolver using the MEC method, while [19] studies the performance of a linear resolver with the winding function approach. While all the mentioned references study the longitudinal end effect, Reference [20] addresses transverse end effects using a tubular structure. This paper demonstrates that the tubular resolver can be a suitable choice for linear motion. Therefore, a configuration of a variable reluctance resolver is proposed in this paper. Given that this construction compensates for the transverse edge effect, optimization is performed to address the compensation of the longitudinal end effect.
This paper investigates a tubular linear resolver with a variable air-gap length. Performance is evaluated using the MEC method, and the model's validity is verified by comparison with finite element simulation results. The rotor saliency count, a key parameter influencing resolver performance, is analyzed for various configurations, and an

[1] *Department of Electrical Engineering, Iran University of Science and Technology, Tehran, Iran*
[2] Department of *Electrical and Computer Engineering, Isfahan University of Technology, Isfahan, Iran*
**Corresponding author, Email:tootoonchian@iust.ac.ir*

optimal design is experimentally validated. The results confirm the accuracy of the proposed approach.

2. Resolver Design and Configuration Overview

Resolvers consist of two main components: the mover and the stator. In variable reluctance resolvers, the stator contains two sets of windings: the excitation and signal windings. The signal winding is further divided into two categories: sin and cos. Fig.1(a) and (b) show the stator and mover structures of the resolver under investigation, respectively. As illustrated in this figure, the mover features a non-wound solid construction. Owing to its design, the distance between any given point on the mover and the stator varies sinusoidally along the mover's length.

The number of turns in the excitation and signal windings in each stator slot is calculated using the relationships in equations (1) to (3) [4]:

$$T_{exc}(i) = Round\{N_{EMax}\cos((i-1)\pi)\} \quad (1)$$

$$T_{sin}(i) = Round\left\{N_{SMax}\sin P_w\left(\frac{2\pi}{z_s}(i-1)\right)\right\} \quad (2)$$

$$T_{cos}(i) = Round\left\{N_{SMax}\cos P_w\left(\frac{2\pi}{z_s}(i-1)\right)\right\} \quad (3)$$

In these relationships, $T_{exc}(i)$, $T_{sin}(i)$, and $T_{cos}(i)$ represent the number of turns of the excitation winding, the sin signal winding, and the cos signal winding, respectively, for tooth i. N_{EMax} and N_{SMax} are the maximum number of turns for the excitation winding and the signal winding, respectively. P_w is the number of pole pairs of the winding, and z_s is the number of stator slots/teeth. It is worth mentioning that overlapping winding is considered for the proposed resolver, which means that all excitation, sin, and cos windings are present in each slot.

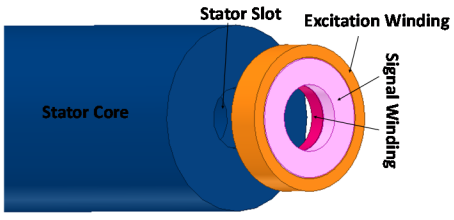

(a)

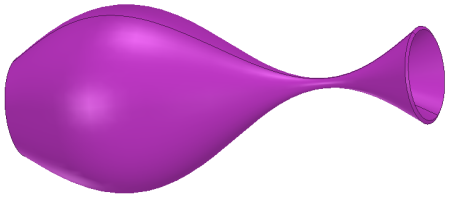

(b)

Fig.1: Proposed resolver configuration a) stator and winding b) mover (variable air-gap)

3. Analytical Modeling of the Resolver

To evaluate the resolver's performance, the Magnetic Equivalent Circuit (MEC) method is utilized. Initially, the reluctances of fixed components, such as the teeth and yoke, are computed. Next, the reluctance of the air gap is determined as a function of the moving part's position, allowing for the calculation of variable reluctances at each time step. Based on the resolver's dimensions and position, the reluctances of various sections are established, forming a reluctance matrix. In developing the proposed model, saturation effects are neglected due to the low flux density in resolvers. Additionally, the model operates under steady-state conditions. Figure 2 illustrates the reluctances of different resolver components.

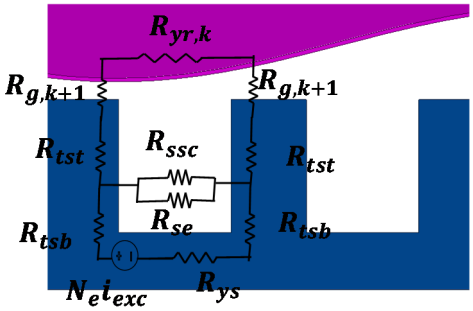

Fig.2: Magnetic equivalent circuit model of proposed resolver

Considering the stator structure, the permeance of the stator yoke is given by [21]:

$$P_{ys} = \mu\pi(r_{is}^2 - r_{os}^2)/y_{zs} \quad (4)$$

In this equation, y_{zs} is the length of a stator tooth and slot, while r_{is} and r_{os} represent the inner and outer radius of the stator, respectively.

The permeance of the stator tooth is also calculated using equations (5) and (6).

$$p_{tsb} = 2\pi w_{st}\mu/\ln\left(\frac{r_{as}}{h_{ss}/2}\right) \quad (5)$$

$$p_{tst} = 2\pi w_{st}\mu/\ln\left(\frac{r_{as}}{r_{os}}\right) \quad (6)$$

Here, w_{st} is the width of the stator tooth, r_{as} is the total height of the yoke plus half the tooth height in the stator, h_{ss} is the height of the stator slot, and r_{os} is the outer radius of the stator.

The reluctances of the stator slots are connected in parallel, so the equivalent permeance of a slot is given by:

$$p_{ss} = \frac{\mu_0\pi}{w_{ss}\times\left(\frac{6d_{ex}^2}{A} + \frac{1}{r_{mine}^2 - r_{is}^2}\right)} \quad (7)$$

Where A can be defined as:

$$A = 3r_{maxe}^4 - 8r_{maxe}^3 r_{mine} + 6r_{maxe}^2 r_{mine}^2 - 4r_{mine}^4 \quad (8)$$

To calculate the reluctance of the variable reluctance section, the mover structure is divided along its length into disks stacked on top of each other. Then, the reluctance of each disk is calculated integrally, and finally, the reluctance of the variable reluctance section in the desired region is determined. Based on the reactance relationship for the disk, the reactance of a differential disk element is first calculated:

$$dR_{yr} = \frac{dz}{\mu\pi(r_{or}^2 - (g(z) + r_{os})^2)} \quad (9)$$

In this equation, r_{or} is the outer radius of the variable reluctance section.
Then, by integrating the above relation over the desired range, the total reactance is calculated according to equation (10):

$$R_{yr,k} = \int_{(k-1)\frac{L_{eff}}{Z}}^{k\frac{L_{eff}}{Z}} dR_{yr} \quad (10)$$

where $R_{yr,k}$ represents the reactance of the mover yoke in part k, and L_{eff} is the effective length of the mover.
The reciprocal of the obtained value represents the reluctance of the moving section over the desired length range. To calculate the reluctance of the air gap, the shape of the air gap is first simplified by the S-C mapping, and then the reluctance of each element is calculated using the following relation [14]:

$$dp_{g,i} = \frac{\mu_0 w}{l} r d\varphi \quad (11)$$

By calculating the reluctances of the various sections, the reluctance matrix is computed according to equation (12):

$$M = \begin{bmatrix} [M_{yr}] & [M_{yrtr}] & 0 & 0 \\ [M_{yrtr}] & [M_{tr}] + [M_{trts}] & [\rho_{ag}]^T & 0 \\ 0 & -[\rho_{ag}]^T & [M_{ts}] + [M_{tstr}] & [M_{ysts}] \\ 0 & 0 & -[M_{ysts}] & [M_{ys}] \end{bmatrix} \quad (12)$$

In this equation, the elements of the desired matrix $[M_{ij}]$ represent the reluctances connected to the nodes i and j in the magnetic equivalent circuit of the resolver. In the next step, the magnetic potential at the different nodes is calculated using equations (13) and (14).

$$[\mathcal{F}_{tr}] = [T]i \quad (13)$$

$$A = [[A_{yr}][A_{tr}][A_{ts}][A_{ys}]]^T = M^{-1} \times [\begin{matrix} 0 \\ [\mathcal{F}_{tr}] \end{matrix}] \quad (14)$$

Then, the flux passing through each stator tooth is calculated using equation (15).

$$[\varphi_{ts}] = [M_{ysts}] \times ([A_{ts}] - [A_{ys}]) \quad (15)$$

After calculating the flux passing through the stator teeth, the induced voltage in the sin and cos signal windings is calculated:

$$\lambda_s = [T_s] \times [\varphi_{ts}] \quad (16)$$
$$\lambda_c = [T_c] \times [\varphi_{ts}] \quad (17)$$
$$v_s = d\lambda_s/dt \quad (18)$$
$$v_c = d\lambda_c/dt \quad (19)$$

Fig. 3 shows the induced voltages in the signal windings based on the performed modeling.

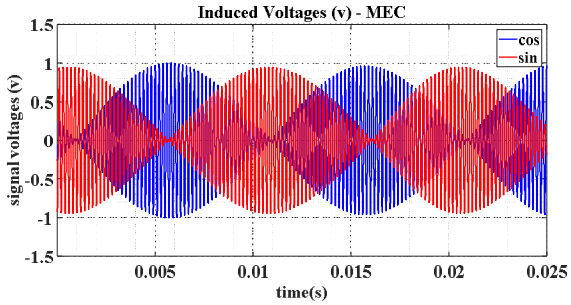

Fig. 3: Induced Voltages in Signal Windings Based on the Magnetic Equivalent Circuit (MEC) Method

As observed from the above figure, the performance of the designed sensor is as expected. To verify the accuracy of the modeling, the resolver under investigation is then simulated using the Ansys Electronics Desktop software, and the results of the modeling are validated.

A. Validation of Proposed Model

Finite Element Simulation is the most accurate method for analyzing the performance of electrical machines. However, due to the significant simulation time, it is generally used for initial investigation and validation of the conducted modeling. In this section, to validate the performed modeling, the results obtained from the modeling are compared with the results from the simulation. Fig. 4 shows the voltages obtained from the finite element simulation. Considering the long simulation time required for finite element analysis and to increase the simulation speed, a lower excitation frequency is selected compared to the Magnetic Equivalent Circuit method.

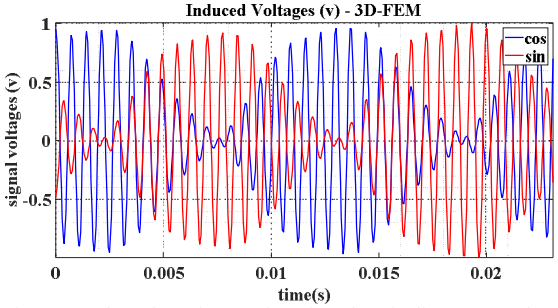

Fig. 4: Induced Voltages in Signal Windings Based on Finite Element Method Simulation

As seen in the figure, the results from the finite element simulation and the modeling are consistent in terms of voltage amplitude and signal phase. Therefore, the

modeling is highly accurate, and it can be used for further investigation of other parameters. Table. 1 shows the comparison between proposed analytical model and FEM.

Table.1: comparison of proposed analytical method and FEM

	Analytical Method	FEM
Voltage amplitude	954 mv	963 mv

B. Alternative Configurations

As observed in Fig. 1, the excitation and signal windings are placed in the horizontal grooves of the stator, which are located on its inner surface. The presence of windings in the inner grooves complicates the manufacturing process. Therefore, if the resolver structure could be modified to an external stator, the manufacturing process would become simpler. Fig. 5 illustrates the external stator structure of the resolver under investigation.

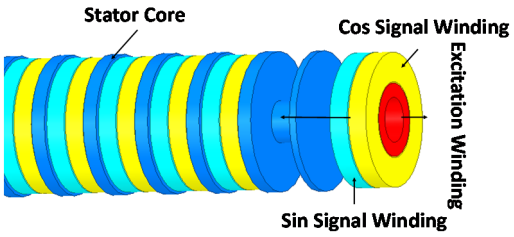

Fig. 5: Internal Stator Structure of the Resolver Under Study

As shown in Fig. 5, the winding process in the external stator structure is significantly easier. In both examined structures, the length of the toothed section is long, while the length of the variable reluctance section is short. Since in variable reluctance resolvers, one section lacks windings, simplifying the manufacturing process allows for making the toothed section shorter and the winding-free section longer. Fig. 6 (a) and (b) display the resolver structure with long variable reluctance sections placed internally and externally. Among the configurations explored, the external stator resolver with a long variable reluctance section offers the simplest and most cost-effective manufacturing process. Therefore, it is chosen as the preferred structure for optimization studies. By altering the dimensions of the resolver in the magnetic equivalent circuit model, the behavior of the external stator resolver with the long variable reluctance section can be examined. Fig. 7 shows the induced voltages in the signal windings of the external stator resolver with the long variable reluctance section.

As observed in Fig. 7, the change from an internal to an external stator and the switch to a variable reluctance section does not significantly impact the induced voltages. Fig. 8 displays the position error for the resolver under investigation. To determine the measurement error, the peak values of the signals are first computed using MATLAB software, and then the calculated position is compared with the actual position, determined using speed and time by dividing the signal amplitudes and applying the inverse tangent function.

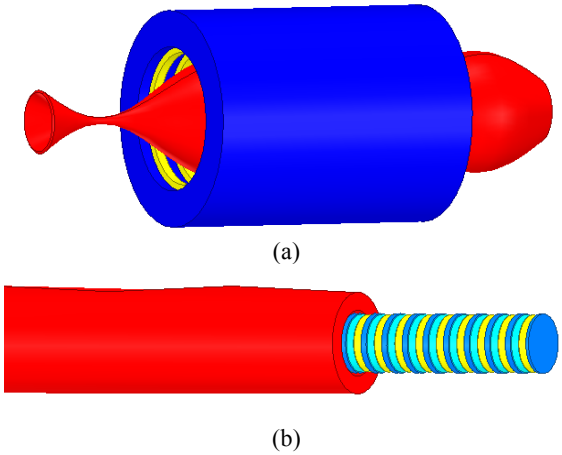

(a)

(b)

Fig.6: Resolver Structure with Long Variable Reluctance Section a) Outer Stator b) Inner Stator

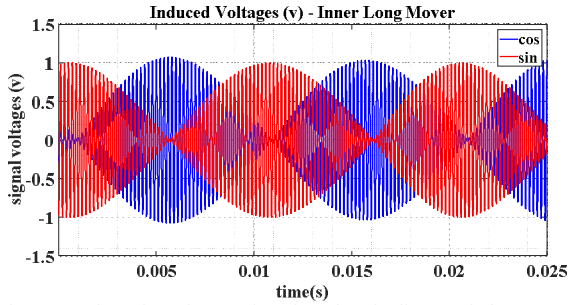

Fig. 7: Induced Voltages in Signal Windings of the Inner Stator Structure with Long Variable Reluctance Section

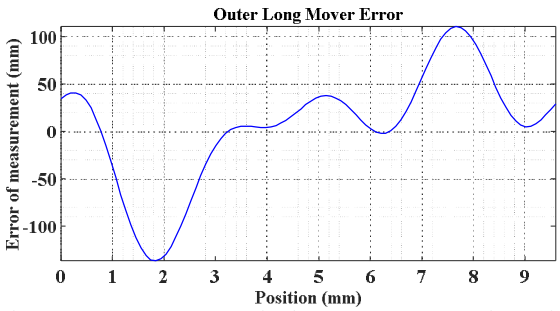

Fig. 8: Measurement Error in the Inner Stator Resolver with Long Variable Reluctance Section

4- End Effect

Due to the asymmetry in the magnetic equivalent circuit of linear machines, their performance is influenced by longitudinal end effects. In resolvers, the presence of these end effects leads to an increase in measurement errors. Therefore, it is crucial to develop methods that can compensate for these end effects, reducing the resulting errors. In the following section, to minimize measurement error, optimization of the variable reluctance section

structure of the resolver is carried out using the magnetic equivalent circuit method.

4-1- Optimization

In variable reluctance resolvers with an air gap length, modifying the number of protrusions in the variable reluctance section alters the number of poles, thus impacting the resolver's performance [6]. In the resolver under study, to reduce the end effect and improve accuracy, the number of protrusions is varied from 1 to 11. The measurement accuracy of the resolver is then evaluated for each configuration [15]. Fig. 9 (a) and (b) show the maximum and average absolute measurement error of the resolver as the number of mover protrusions changes. As observed in these figures, among the various configurations, the mover with five protrusions provides the highest accuracy and the lowest error.

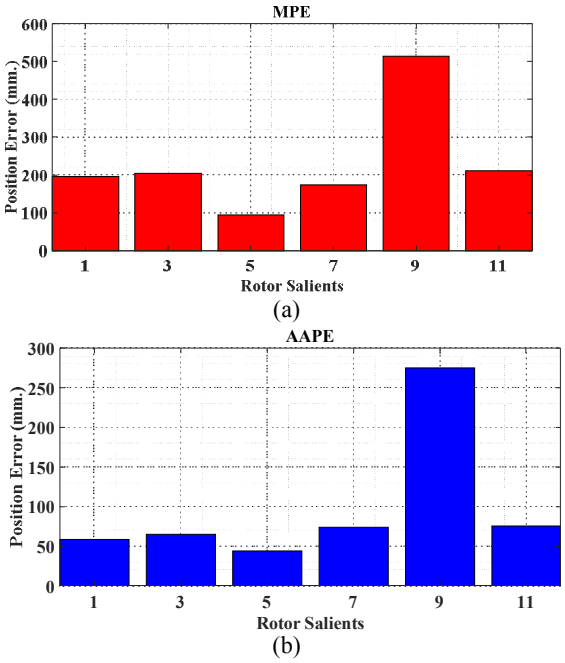

Fig. 9: Measurement Error for Different Numbers of Projections a) Maximum Position Error (MPE), b) Average of Absolute Position Error (AAPE)

Fig. 10 displays the physical structure of the variable reluctance section with five protrusions.

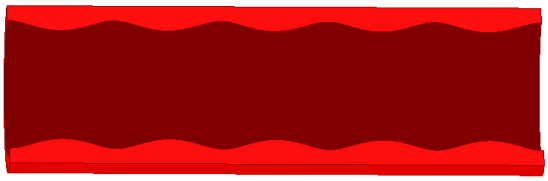

Fig. 10: Mover Structure with Five Projections

Given the increased accuracy in the resolver with a variable reluctance section featuring five projections, this structure is chosen for the construction of the practical prototype.

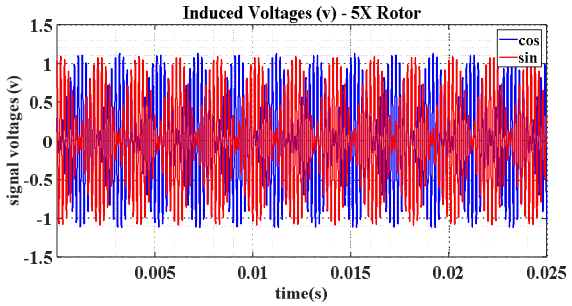

Fig. 11: Induced Voltages in Signal Windings of the Resolver with Five Projections

5. Practical Prototype Construction

To evaluate the performance of the resolver, a practical prototype was built and tested. Based on the optimization results, the tubular resolver with five projections was constructed as the optimal resolver. Fig.12 shows the constructed resolver. It is important to note that, in order to simplify the winding process, the internal stator structure was selected for the construction of the practical prototype. As illustrated in Fig. 12(b), the stator features excitation and signal windings on its outer face. The mover, in contrast, has no saliencies on its outer face; instead, its saliencies are positioned on the inner face. Furthermore, the mover is designed to be longer than the stator.

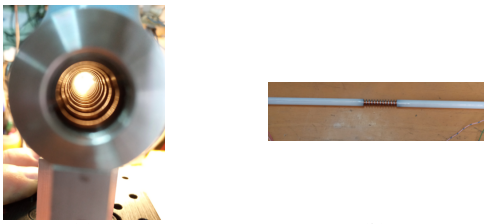

(a) (b)

Fig. 12: Practical prototype of the inner stator resolver with five projections a) Slotted section b) Reluctance variation section

As depicted, the test system includes a function generator supplying a 5 kHz excitation voltage. Linear motion is achieved using a DC motor powered by a DC source. The induced voltages in the signal windings are transmitted to MATLAB software, where signal envelopes are computed. The resolver-determined position is calculated by dividing the envelopes of the two signals and applying the arctangent function. To measure the resolver's positioning error, the calculated position is compared to the position provided by a linear encoder.

Experimental results indicate an average absolute measurement error of 47 µm, closely matching the modeled result of 43.6 µm for the resolver with five projections. This demonstrates strong agreement between the modeling and practical prototype results.

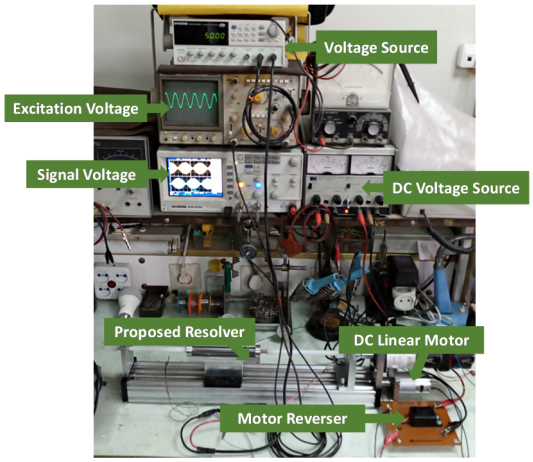

Fig.13: Experimental test

6. Conclusion

In this study, the structure of a tubular linear variable reluctance resolver with varying air gap lengths was investigated. A magnetic equivalent circuit (MEC) method was employed to evaluate the resolver's performance. The accuracy of the MEC model was validated by comparing its results with those obtained from finite element method (FEM) simulations.

Given the high computational speed of the proposed analytical method (MEC), various resolver configurations, including long mover and outer mover designs, were analyzed. Taking into account both accuracy and manufacturability, the optimal configuration was selected.

Given the impact of mover protrusion count on the performance of variable reluctance resolvers with air gap length variation, the measurement error was analyzed for different numbers of mover protrusions. A comparison of errors across various resolver configurations revealed that the resolver with five protrusions exhibited the lowest error, with an absolute average position error of 43.6 μm. Consequently, this configuration was selected as the optimal design, fabricated, and subjected to practical testing.

REFERENCES

[1] X. Ge, Z. Q. Zhu, R. Ren, J. T. Chen "A Novel variable reluctance resolver for HEV/EV applications", *IEEE Trans. Ind. Appl.*, Vol. 52, no. 4, pp. 2872 -2880, July-Aug. 2016

[2] C. Jin, I. Jang, J. Bae, J. Lee, W. Kim, "Proposal of improved winding method for VR resolver", *IEEE Trans. Magn.*, vol. 51, no. 3, Mar. 2015

[3] A. Murray, B. Hare, and A. Hirao, "Resolver position sensing system with integrated fault detection for automotive applications", *Proc. IEEE Sensors*, vol. 2, pp. 864-869, Jun. 2002.

[4] M. Onsal, Y. Demir and M. Aydin, "Comparison of Concentrated and Distributed Winding Configurations on the Position Error for a Conventional Wound-Rotor Resolver," in IEEE Transactions on Magnetics, vol. 59, no. 11, pp. 1-5, Nov. 2023, Art no. 8205405, doi: 10.1109/TMAG.2023.3305749.

[5] H. Saneie, Z. Nasiri-Gheidari, and A. Belahcen, "On the Field-Reconstruction Method for Electromagnetic Modeling of Resolvers," in IEEE Transactions on Instrumentation and Measurement, vol. 72, pp. 1-8, 2023, Art no. 9000608, doi: 10.1109/TIM.2022.3224527.

[6] X. Ge, Z. Q. Zhu, "A novel design of rotor contour for variable reluctance resolver by injecting auxiliary air-gap permeance harmonics", *IEEE Trans. Energy Conversion*, vol. 31, no. 1, pp. 345-353, March 2016

[7] X. Ge, Z. Q. Zhu, R. Ren, J. T. Chen, "A novel variable reluctance resolver with non-overlapping tooth-coil windings", *IEEE Trans. Energy Convers.*, vol. 30, no. 2, pp. 784-794, May 2015

[8] X. Ge, Z. Q. Zhu, R. Ren and J. T. Chen, "Analysis of Windings in Variable Reluctance Resolver," *IEEE Trans., Magn.*, vol. 51, no. 5, pp. 1-10, May 2015

[9] K. Kim, "Analysis on the characteristics of variable reluctance resolver considering uneven magnetic fields," *IEEE Trans. On Magnetics*, vol. 49, no. 7, pp. 3858-3861, Jul. 2013

[10] Zare, F., Z. Nasiri-Gheidari, and F. Tootoonchian. "The effect of winding arrangements on measurement accuracy of sinusoidal rotor resolver under fault conditions." *Measurement* 131 (2019): 162-172.

[11] Saneie, Hamid, Zahra Nasiri-Gheidari, and Farid Tootoonchian. "Design-oriented modelling of axial-flux variable-reluctance resolver based on magnetic equivalent circuits and Schwarz–Christoffel mapping." *IEEE Transactions on Industrial Electronics* 65.5 (2017): 4322-4330.

[12] Nasiri-Gheidari, Zahra, and Farid Tootoonchian. "Axial flux resolver design techniques for minimizing position error due to static eccentricities." *IEEE Sensors Journal* 15.7 (2015): 4027-4034.

[13] Nasiri-Gheidari, Zahra. "Design, analysis, and prototyping of a new wound-rotor axial flux brushless resolver." *IEEE Transactions on Energy Conversion* 32.1 (2016): 276-283.

[14] Z. Nasiri-Gheidari, "Design, Performance Analysis, and Prototyping of Linear Resolvers", *IEEE Trans. on Energy Conversion,* Vol. 32, no. 4, pp. 1-10, Dec. 2017

[15] A. Ramezannezhad, P. Naderi and L. Vandevelde, "A Novel Method for Accuracy Improvement of Variable Reluctance Linear Resolvers," in *IEEE Sensors Journal*, vol. 22, no. 19, pp. 18409-18417, 1 Oct.1, 2022, doi: 10.1109/JSEN.2022.3199807.

[16] Farrokh, Fariba, et al. "A 2D hybrid analytical electromagnetic model of the dual□stator axial□field flux□switching permanent magnet motor." *IET Electric Power Applications* 18.2 (2024): 252-264.

[17] Farrokh, Fariba, et al. "Fast 2-D analytical model for axial-field flux-switching bar-permanent magnet motor." *IEEE Transactions on Magnetics* (2024).

[18] S. A. Seyed-Bouzari, H. Saneie and Z. Nasiri-Gheidari, "Analysis and Compensation of the Longitudinal End Effect in Variable Reluctance Linear Resolvers Using Magnetic Equivalent Circuit Model," in *IEEE Transactions on Transportation Electrification*, vol. 9, no. 3, pp. 3970-3977, Sept. 2023, doi: 10.1109/TTE.2023.3239500.

[19] M. Bahari, R. Alipour-Sarabi, Z. Nasiri-Gheidari, and F. Tootoonchian, "Proposal of Winding Function Model for Geometrical Optimization of Linear Sinusoidal Area Resolver", *IEEE Sensors Journal*, vol. 19 no. 14, pp. 5506 – 5513, July 15, 15 2019

[20] F. Zare, F. Tootoonchian, "Design of a Linear Tubular Resolver with the aim of eliminating the transverse edge effect", 2nd International Conferences on Electric Machines and Drives (ICEMD), Sabzevar, Iran, 2022

[21] Keyvannia, Ali, Fateme Zare, and Farid Tootoonchian. "Analytical modeling of variable-reluctance tubular resolver based on magnetic equivalent circuit and conformal mapping." IEEE Transactions on Instrumentation and Measurement 70 (2021): 1-8.